Soil Moisture Active Passive (SMAP) Project

Algorithm Theoretical Basis Document

SMAP L1C Radiometer Data Product (L1C_TB)

Revision B

PREPARED BY:

Steven Chan
Jet Propulsion Laboratory
SMAP Algorithm Development Team Lead for
L1C_TB Data Product

Date

Eni Njoku
Jet Propulsion Laboratory
SMAP Algorithm Development Team for
L1C_TB Data Product

Date

Andreas Colliander
Jet Propulsion Laboratory
SMAP Algorithm Development Team for
L1C_TB Data Product

Date

APPROVED BY:

Simon Yueh, JPL
SMAP Project Scientist

Date

October 14, 2015
JPL D-53053

Jet Propulsion Laboratory
California Institute of Technology

Soil Moisture Active Passive (SMAP)

Algorithm Theoretical Basis Document

Level 1C Radiometer Data Product

Revision B
October 14, 2015

Steven Chan
Eni Njoku
Andreas Colliander

Jet Propulsion Laboratory
California Institute of Technology
Pasadena, CA

Jet Propulsion Laboratory
California Institute of Technology

The research was carried out at the Jet Propulsion Laboratory, California Institute of Technology, under a contract with the National Aeronautics and Space Administration.

TABLE OF CONTENTS

ACRONYMS & ABBREVIATIONS

ADT	Algorithm Development Team
ATBD	Algorithm Theoretical Basis Document
Cal/Val	Calibration and Validation
DAAC	Distributed Active Archive Center
DIB	Drop-in-Bucket
EASE Grid	Equal-Area Scalable Earth Grid
GSFC	Goddard Space Flight Center
IDS	Inverse Distance Squared
IFOV	Instantaneous Field Of View
JPL	Jet Propulsion Laboratory
L1B_TB	Level 1B Brightness Temperature
L1C_S0_HiRes	Level 1C Sigma-0 High Resolution
L1C_TB	Level 1C Brightness Temperature
L2_SM_P	Level 2 Soil Moisture Passive
L4_SM	Level 4 Soil Moisture
NDVI	Normalized Difference Vegetation Index
NEDT	Noise Equivalent Delta-T
NN	Nearest Neighbor
NSIDC	National Snow and Ice Data Center
PDR	Preliminary Design Review
SDS	Science Data System
SDT	Science Definition Team
SOM	Space-Oblique Mercator
SMAP	Soil Moisture Active Passive
SPS	Science Production System
TB	Brightness Temperature
TBD	To Be Determined

1. Introduction

1.1 Purpose

This document provides the theoretical basis and computational approaches for generating the SMAP Level 1C Radiometer Data Product (L1C_TB). In addition, it describes the major output data fields, data volume, computational requirements, and calibration and validation (Cal/Val) criteria for the product.

1.2 Scope and Objectives

SMAP Level 1 brightness temperature (TB) data products are available at Level 1B [1] and Level 1C. The Level 1B data product (L1B_TB) contains calibrated time-ordered TB data, while the Level 1C data product (L1C_TB) contains gridded TB data. The Level 1C processing re-maps the L1B_TB data to an Earth-fixed grid to provide the operational product used for generating higher-level products.

2. Soil Moisture Active Passive (SMAP) Mission

2.1 Background and Science Objectives

The National Research Council's (NRC) Decadal Survey, Earth Science and Applications from Space: National Imperatives for the Next Decade and Beyond, was released in 2007 after a two-year study commissioned by NASA, NOAA, and USGS to provide them with prioritization recommendations for space-based Earth observation programs [2]. Factors including scientific value, societal benefit and technical maturity of mission concepts were considered as criteria. SMAP data products have high science value and provide data towards improving many natural hazards applications. Furthermore SMAP draws on the significant design and risk-reduction heritage of the Hydrosphere State (Hydros) mission concept [3]. For these reasons, the NRC report placed SMAP in the first tier of missions in its survey. In 2008 NASA announced the formation of the SMAP project as a joint effort of NASA's Jet Propulsion Laboratory (JPL) and Goddard Space Flight Center (GSFC), with project management responsibilities at JPL [4]. The target launch date is January 2015.

The SMAP science and applications objectives are to:

- Understand processes that link the terrestrial water, energy and carbon cycles;
- Estimate global water and energy fluxes at the land surface;
- Quantify net carbon flux in boreal landscapes;
- Enhance weather and climate forecast skill;
- Develop improved flood prediction and drought monitoring capability.

2.2 Measurement Approach

Table 1 is a summary of the SMAP instrument functional requirements derived from its science measurement needs. The goal is to combine the attributes of the radar and radiometer observations (in terms of their spatial resolution and sensitivity to soil moisture, surface roughness, and vegetation) to estimate soil moisture at a resolution of 10 km, and freeze-thaw state at a resolution of 1-3 km.

The SMAP instrument incorporates an L-band radar and an L-band radiometer that share a single feedhorn and parabolic mesh reflector. As shown in Fig. 1 the reflector is offset from nadir and rotates about the nadir axis at 14.6 rpm (nominal), providing a conically scanning antenna beam with a surface incidence angle of approximately 40°. The provision of constant incidence angle across the swath simplifies the data processing and enables accurate repeat-pass estimation of soil moisture and freeze/thaw change. The reflector has a diameter of 6 m, providing a radiometer 3-dB antenna footprint of about 40 km. The real-aperture radar footprint is about 30 km, defined by the two-way antenna beamwidth. The real-aperture radar and radiometer data will be collected globally during both ascending and descending passes.

To obtain the desired high spatial resolution the radar employs range and Doppler discrimination. The radar data can be processed to yield resolution enhancement to 1-3 km spatial resolution over the 70% outer parts of the 1000 km swath. Data volume prohibits the downlink of the entire radar data acquisition. Radar measurements that allow high-resolution processing will be collected during the morning overpass over all land regions and extending one swath width over the surrounding oceans. During the evening overpass data poleward of 45° N will be collected and processed as well to support robust detection of landscape freeze/thaw transitions.

Table 1. SMAP Mission Requirements

Scientific Measurement Requirements	Instrument Functional Requirements
Soil Moisture: ~ ±0.04 m^3m^{-3} volumetric accuracy (1-sigma) in the top 5 cm of soil for vegetation water content ≤ 5 kg m^{-2}; Hydrometeorology at ~10 km resolution; Hydroclimatology at ~40 km resolution	L-Band Radiometer (1.41 GHz): Polarization: T_v, T_h, T_3 and T_4 Resolution: 40 km Radiometric Uncertainty*: 1.3 K L-Band Radar (1.26 and 1.29 GHz): Polarization: VV, HH, HV (or VH) Resolution: 10 km Relative accuracy*: 0.5 dB (VV and HH) Constant incidence angle** between 35° and 50°
Freeze/Thaw State: Capture freeze/thaw state transitions in integrated vegetation-soil continuum with two-day precision, at the spatial scale of landscape variability (~3 km).	L-Band Radar (1.26 GHz and 1.29 GHz): Polarization: HH Resolution: 3 km Relative accuracy*: 0.7 dB (1 dB per channel if 2 channels are used) Constant incidence angle** between 35° and 50°
Sample diurnal cycle at consistent time of day (6am/6pm Equator crossing); Global, ~3 day (or more frequent) revisit; Boreal, ~2 day (or more frequent) revisit	Swath Width: ~1000 km Minimize Faraday rotation (degradation factor at L-band)
Observation over minimum of three annual cycles	Baseline three-year mission life

* Includes precision and calibration stability

** Defined without regard to local topographic variation

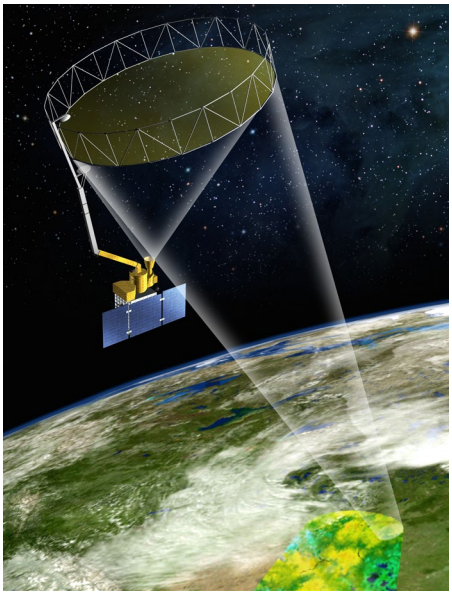

Figure 1. The SMAP observatory is a dedicated spacecraft with a rotating 6-m lightweight deployable mesh reflector. The radar and radiometer share a common feed.

The baseline orbit parameters are:

- Orbit altitude: 685 km (2-3 days average revisit and 8-days exact repeat)
- Inclination: 98 degrees, sun-synchronous
- Local time of ascending node: 6 pm

The SMAP radiometer measures the four Stokes parameters, T_v, T_h, T_3, and T_4 at 1.41 GHz. The T_3-channel measurement can be used to correct for Faraday rotation caused by the ionosphere, although such Faraday rotation is minimized by the selection of the 6am/6pm sun-synchronous SMAP orbit.

At L-band, anthropogenic Radio Frequency Interference (RFI), principally from ground-based surveillance radars, can contaminate both radar and radiometer measurements. Early measurements and results from the SMOS mission indicate that in some regions RFI is present and detectable. The SMAP radar and radiometer electronics and algorithms have been designed to include features to mitigate the effects of RFI. For this purpose, the SMAP radar utilizes selective filters and an adjustable carrier frequency in order to tune to pre-determined RFI-free portions of the spectrum while on orbit. The SMAP radiometer will implement a combination of time and frequency diversity, kurtosis detection, and use of T_4 thresholds to detect and where possible mitigate RFI.

The SMAP planned data products are listed in Table 2. Level 1B and 1C data products are calibrated and geolocated instrument measurements of surface radar backscatter cross-section and brightness temperatures. Level 2 products are half-orbit geophysical retrievals of soil moisture on a fixed Earth grid, based on Level 1 products and ancillary information. Level 3 products are global daily composites of Level 2 surface soil moisture and freeze/thaw state data. Level 4 products are model-derived value-added data products that support key SMAP applications and more directly address the driving science questions.

Table 2. SMAP Data Products Table

Product	Description	Gridding (Resolution)	Latency**	
L1A_Radiometer	Radiometer Data in Time-Order	-	12 hrs	Instrument Data
L1A_Radar	Radar Data in Time-Order	-	12 hrs	
L1B_TB	Radiometer T_B in Time-Order	(36x47 km)	12 hrs	
L1B_S0_LoRes	Low Resolution Radar σ_o in Time-Order	(5x30 km)	12 hrs	
L1C_S0_HiRes	High Resolution Radar σ_o in Half-Orbits	1 km (1-3 km)	12 hrs	
L1C_TB	Radiometer T_B in Half-Orbits	36 km	12 hrs	
L2_SM_A	Soil Moisture (Radar)	3 km	24 hrs	Science Data (Half-Orbit)
L2_SM_P	Soil Moisture (Radiometer)	36 km	24 hrs	
L2_SM_AP	Soil Moisture (Radar + Radiometer)	9 km	24 hrs	
L3_FT_A	Freeze/Thaw State (Radar)	3 km	50 hrs	Science Data (Daily Composite)
L3_SM_A	Soil Moisture (Radar)	3 km	50 hrs	
L3_SM_P	Soil Moisture (Radiometer)	36 km	50 hrs	
L3_SM_AP	Soil Moisture (Radar + Radiometer)	9 km	50 hrs	
L4_SM	Soil Moisture (Surface and Root Zone)	9 km	7 days	Science Value-Added
L4_C	Carbon Net Ecosystem Exchange (NEE)	9 km	14 days	

3. Product Description

3.1 Overview

To generate the L1C_TB data product the processing software ingests the L1B_TB product data, and based on the geometry and geolocation information the data are re-mapped onto an Earth-fixed grid using a gridding algorithm. The L1C_TB data product is thus simply a gridded version of the L1B_TB data product sharing the same major output data fields and data granularity (i.e., one half orbit per file).

The L1C_TB product is planned for use in generating the higher-level (L2-L4) soil moisture data products. The advantage of using the L1C_TB product is that ancillary data on land characteristics required by the L2-L4 algorithms (e.g., soil texture, static water fraction, land cover class, etc.) can be pre-gridded off-line and the retrievals performed with all data values registered to the same grid. A disadvantage is that some spatial resolution is inevitably lost in the gridding process. Both the L1B_TB and L1C_TB data products will be archived and made available to users.

The Earth-fixed grid used for the L1C_TB data product is a 36-km global grid based on the Equal-Area Scalable Earth Grid 2.0 (EASEv2) projection developed by the NSIDC [5,6]. The same projection is used for generating other higher-level (L2-L4) data products at the resolutions required for those products.

In each L1C_TB granule, data from the fore- and aft-look portions of the 360° antenna scan are stored separately. This separation provides potential benefits to radiometric analyses over regions where there is strong TB azimuthal dependence.

In post-launch operational processing the L1C_TB data product will be generated in the SMAP Science Data System (SDS) using the selected baseline gridding algorithm. A limited number of alternate gridding algorithms will also be coded prior to launch for comparison and evaluation as part of the Cal/Val activities.

3.2 Processing Description

The L1C_TB data product is derived from the L1B_TB data product. Figure 2 shows the processing scheme. During operational processing, the L1C_TB processor applies the baseline gridding algorithm (Section 4) to a half-orbit L1B_TB granule and converts it into the corresponding L1C_TB granule. The L1C_TB processing is essentially a re-mapping of time-ordered swath data onto a grid. Both the input L1B_TB and output L1C_TB data share the same granularity (i.e., one half orbit per file). There is no geophysical processing performed (e.g. no TB correction for fractional water within the antenna FOV).

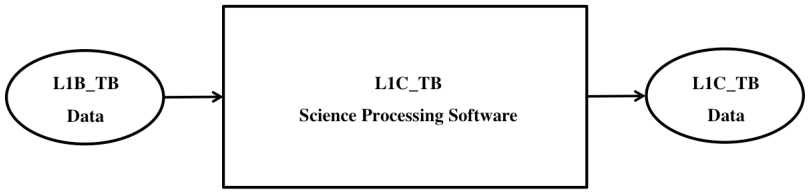

Figure 2. Overview of L1C_TB processing. During operational processing, the L1C_TB software ingests an input L1B_TB granule and converts it into an output L1C_TB granule using a gridding algorithm. The resulting L1C_TB data are referenced on the 36-km global EASE grid.

The processing computations involve the following steps:

1. Transform (lat,lon) of input data to decimal values of 36-km EASEv2 row and column indices
2. Identify T_B data samples within a given grid cell (or nearest the grid cell center, or within a given radial distance from the grid cell center, according to the gridding algorithm to be used)
3. Apply the gridding algorithm to these T_B data samples
4. Assign the computed result to the grid cell
5. Repeat Steps 2−4 above for all other grid cells.

The same gridding algorithm is applied to the brightness temperatures and other applicable parameters in the L1B_TB output data product (e.g. latitude, longitude, azimuth angle, incidence angle, reflected sun angles, etc.) as appropriate. Individual L1B_TB quality flags, on the other hand, need to be combined using other strategies and encoded as integers as described in Section 4.4.

3.2.1 Input (L1B_TB)

The L1B_TB data are organized in time order as described in the SMAP L1B_TB Algorithm Theoretical Basis Document (ATBD) [1]. A typical L1B_TB granule contains radiometric brightness

temperature values and associated time tags, geolocation data, incidence angles, azimuth angles, reflected sun angles, and quality flags. These data fields are either provided at, or are sub-sampled to, individual T_B data sample locations.

The time interval between successive T_B data samples for a given polarization channel (T_h, T_v, T_3 or T_4) is nominally 16.8 milliseconds [1]. When projected on the Earth surface, the L1B_TB samples trace out a helical scan pattern illustrated in Fig. 3. The red ellipses in the figure depict the 3-dB instantaneous field-of-view (IFOV) footprints of the antenna beam. Because there is significant over-sampling in the along-scan direction, only every third footprint along the scan is shown. Several 360-degree scans are shown to illustrate the overlap in the along-track direction. A more detailed depiction of the radiometer footprints relative to the grid is shown in Fig. 7 (Section 4).

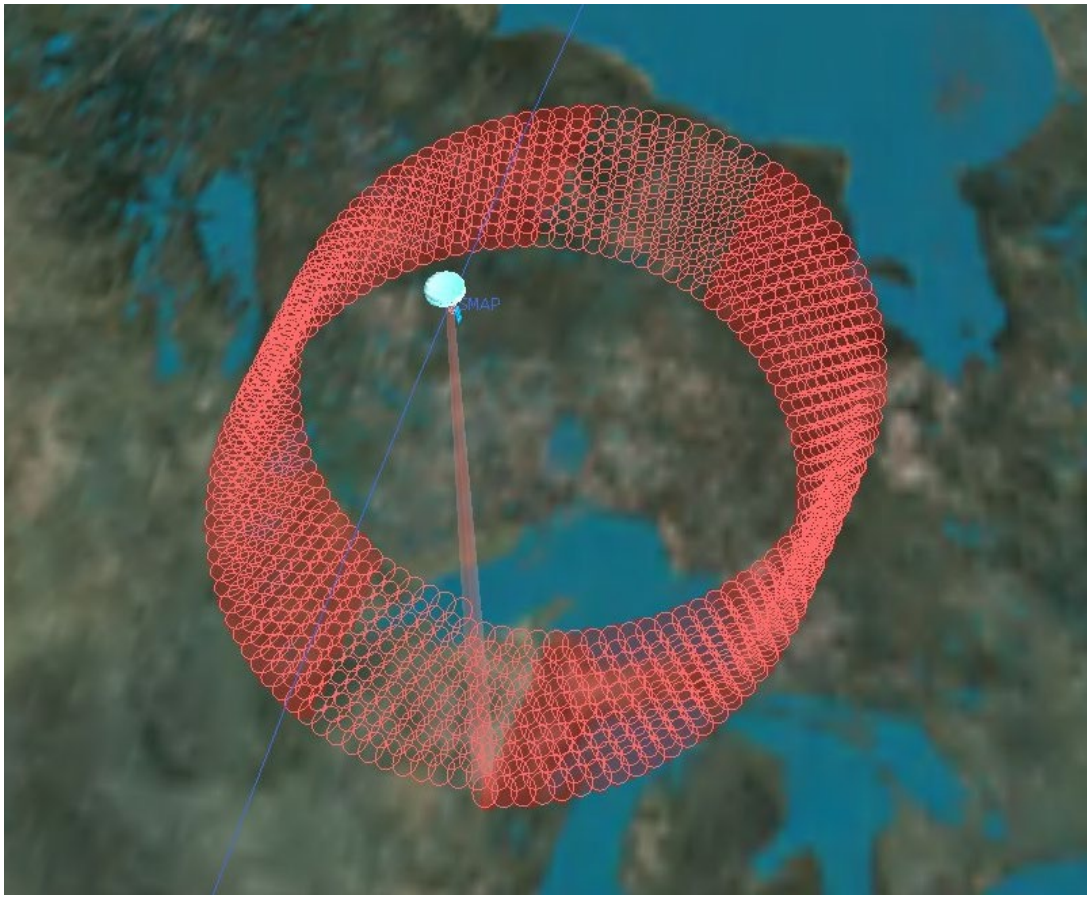

Figure 3. SMAP radiometer 3-dB instantaneous field-of-view footprints (red ellipses) mapped out by the helical scan pattern. For display clarity, only every third footprint along the scan is shown. For the nominal SMAP orbit altitude and antenna rotation rate the maximum distance between footprint centers along the groundtrack is approximately 28 km.

3.2.2 Output (L1C_TB)

The L1C_TB data product contains gridded TB data on three 36-km EASE Grid projections: global projection, north polar projection, and south polar projection [6]. This particular family of 36-km

projections, together with its higher-resolution counterparts (1 km, 3 km, and 9 km), was developed by NSIDC to satisfy the grid requirements of the SMAP science data products. Because the EASE-Grid projection suite has been used for several other passive microwave datasets (e.g. SMMR, SSM/I, and AMSR-E), SMAP's adoption of it helps to promote continuity of data formats and re-use of legacy visualization and extraction software tools.

The EASE-Grid family of projections has a flexible formulation. By adjusting a scale parameter, it is possible to generate a family of multi-resolution grids that nest within one another. Perfect nesting occurs when the dimensions of larger grid cells are chosen to be integer multiples of those of smaller grid cells, as shown in Fig. 4 where smaller grid cells (e.g. 3 km or 9 km) nest completely within larger grid cells (36 km). This perfect nesting feature provides a common colocation scheme for applying and analyzing SMAP L2-L4 algorithms and data products at 3, 9, or 36 km.

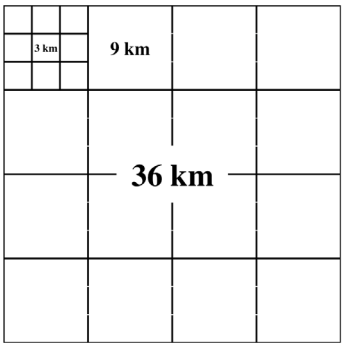

Figure 4. Perfect grid nesting – Smaller grid cells nest within larger grid cells when grid dimensions of larger cells are chosen to be integer multiples of those of smaller cells.

To illustrate the appearance of data projected on the EASE Grid of different resolutions, Figure 5 shows Normalized Difference Vegetation Index (NDVI) images on the 36-, 9-, and 3-km EASE grids. All three images have the same aspect ratio due to perfect nesting among cells of different grid resolutions. As grid resolution increases (i.e., grid dimensions become smaller) more spatial detail becomes visible.

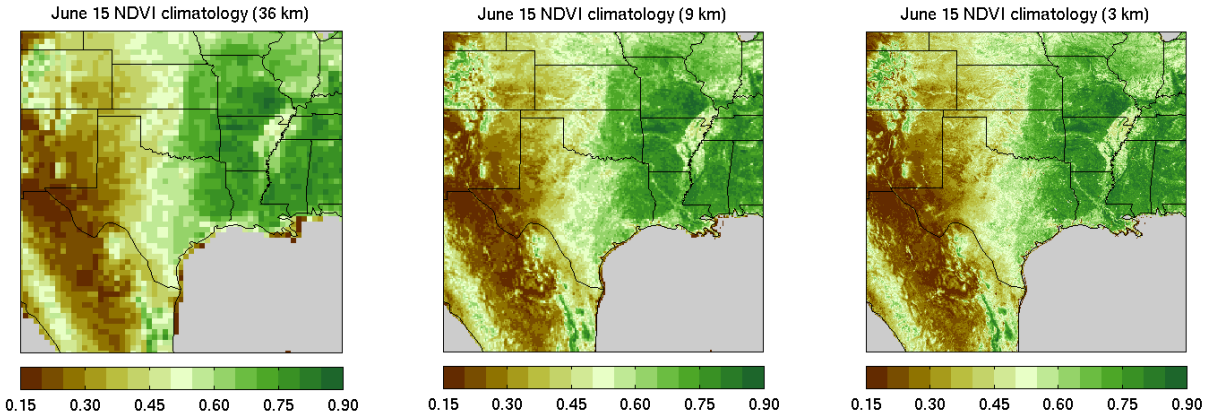

Figure 5. NDVI images at 36-, 9-, and 3-km grid resolutions. Perfect nesting among the three grids enables consistent and convenient analysis and display of multi-resolution data.

A complete description of the contents of the L1C_TB data product is contained in the SMAP L1C_TB Data Product Specification document (a SMAP project document available on request) [18]. Table 3 describes a subset of the major output fields currently included in the L1C_TB product.

Table 3: Primary output fields of a descending half-orbit L1C_TB granule (an ascending half-orbit L1C_TB granule would contain identical output fields). The fields are grouped into two azimuth groups: fore-look direction and aft-look direction. Each category contains data fields derived from T_B samples acquired within the respective fore and aft antenna scan angle ranges.

Granule	Azimuth Direction	Output Fields	Size	Data Precision	Units	Method*
Descending half orbit	Fore-look L1C_TB	Time in J2000 second	K □ 1	float64	Second	1
		Time in J2000 text	K □ 24	string	N\A	1
		Row index	K □ 1	uint32	N\A	2
		Column index	K □ 1	uint32	N\A	2
		Center latitude	K □ 1	float32	Degree	2
		Center longitude	K □ 1	float32	Degree	2
		Centroid latitude	K □ 1	float32	Degree	1
		Centroid longitude	K □ 1	float32	Degree	1
		Antenna scan angle	K □ 1	float32	Degree	1
		Incidence angle	K □ 1	float32	Degree	1
		Solar specular elevation angle	K □ 1	float32	Degree	1
		Solar specular azimuth angle	K □ 1	float32	Degree	1
		T_h	K □ 1	float32	Kelvin	1
		T_v	K □ 1	float32	Kelvin	1
		T_3	K □ 1	float32	Kelvin	1
		T_4	K □ 1	float32	Kelvin	1
		Number of T_h	K □ 1	uint32	N\A	1
		Number of T_v	K □ 1	uint32	N\A	1
		Number of T_3	K □ 1	uint32	N\A	1
		Number of T_4	K □ 1	uint32	N\A	1
		T_h NEDT	K □ 1	float32	Kelvin	1
		T_v NEDT	K □ 1	float32	Kelvin	1
		T_3 NEDT	K □ 1	float32	Kelvin	1
		T_4 NEDT	K □ 1	float32	Kelvin	1
		T_h quality flag	K □ 1	uint32	N\A	3
		T_v quality flag	K □ 1	uint32	N\A	3
		T_3 quality flag	K □ 1	uint32	N\A	3
		T_4 quality flag	K □ 1	uint32	N\A	3
	Aft-look L1C_TB	Time in J2000 second	K □ 1	float64	Second	1
		Time in J2000 text	K □ 24	string	N\A	1
		Row index	K □ 1	uint32	N\A	2
		Column index	K □ 1	uint32	N\A	2
		Center latitude	K □ 1	float32	Degree	2
		Center longitude	K □ 1	float32	Degree	2
		Centroid latitude	K □ 1	float32	Degree	1
		Centroid longitude	K □ 1	float32	Degree	1
		Antenna scan angle	K □ 1	float32	Degree	1
		Incidence angle	K □ 1	float32	Degree	1
		Solar specular elevation angle	K □ 1	float32	Degree	1
		Solar specular azimuth angle	K □ 1	float32	Degree	1

		T_h	K □ 1	float32	Kelvin	1
		T_v	K □ 1	float32	Kelvin	1
		T_3	K □ 1	float32	Kelvin	1
		T_4	K □ 1	float32	Kelvin	1
		Number of T_h	K □ 1	uint32	N\A	1
		Number of T_v	K □ 1	uint32	N\A	1
		Number of T_3	K □ 1	uint32	N\A	1
		Number of T_4	K □ 1	uint32	N\A	1
		T_h NEDT	K □ 1	float32	Kelvin	1
		T_v NEDT	K □ 1	float32	Kelvin	1
		T_3 NEDT	K □ 1	float32	Kelvin	1
		T_4 NEDT	K □ 1	float32	Kelvin	1
		T_h quality flag	K □ 1	uint32	N\A	3
		T_v quality flag	K □ 1	uint32	N\A	3
		T_3 quality flag	K □ 1	uint32	N\A	3
		T_4 quality flag	K □ 1	uint32	N\A	3

* Method:

1. Computed by gridding algorithm
2. From EASE Grid array definition
3. Thresholds were determined uniquely for each flag bit

3.2.3 EASE Grid Projections

As discussed in [5, 21] the EASE Grid consists of a set of three equal-area projections: the global cylindrical equal-area (CEA), and the Northern and Southern hemisphere azimuthal equal area (AEA) projections (see Fig. 6).

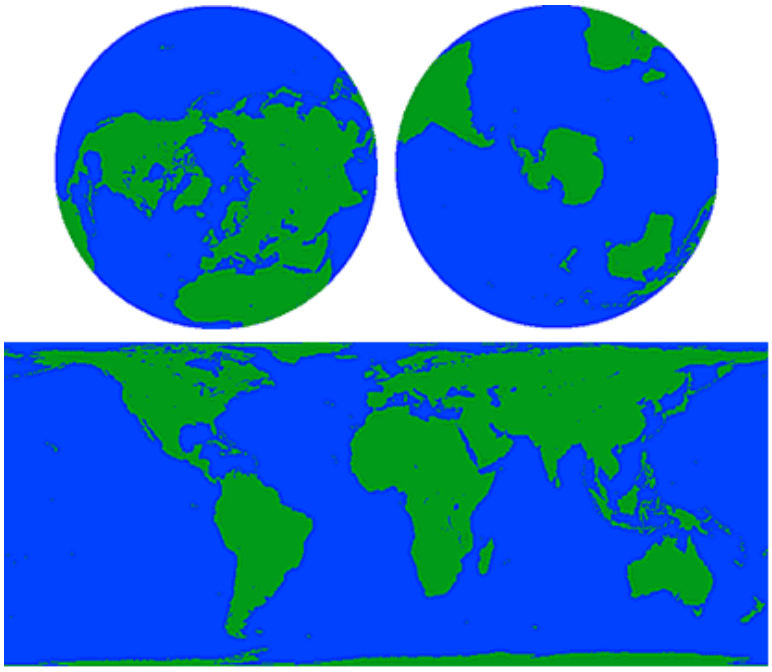

Figure 6. The EASE-Grid Projections [5]. Northern Hemisphere (top left), Southern Hemisphere (top right) and global (bottom). Although these figures describe the original EASE-Grid formulation, they are also valid for the

visualization of the newer EASE-Grid 2.0 formulation [20], which was adopted as the baseline map projection by SMAP (Courtesy of the National Snow and Ice Data Center).

The L1C_TB data product includes output files in each of these three projections. Each file will include the data contents shown in Table 3. Users will be able to build up daily, weekly, monthly, or any time-duration maps in each of these projections by simple compositing (averaging, last-in, etc.) of the individual half-orbit granules. This is anticipated to be a flexible capability for subsequent data analysis and application development.

4. Gridding Algorithms

The SMAP antenna beam traces out a helical scan pattern on the Earth surface. The locations of the L1B_TB data samples and 3-dB footprints on a 36-km EASE Grid are illustrated to the correct scale in Fig. 7. L1B_TB data samples that fall within a given grid cell (red and green dots within the black rectangle in Fig. 7) could come from both fore-look scans (the two convex upward arcs) and aft-look scans (the one concave downward arc). The green dot indicates the sample closest to the grid cell center. Although the 3-dB footprint of each sample point is shown as a red ellipse it should be noted that a significant percentage[1] of the contribution to the brightness temperature of that sample point comes from outside the 3-dB region. This is because the antenna pattern correction performed in the L1B_TB processing [1] corrects only for radiation entering from outside the main beam region (2½ times the 3-dB beamwidth).

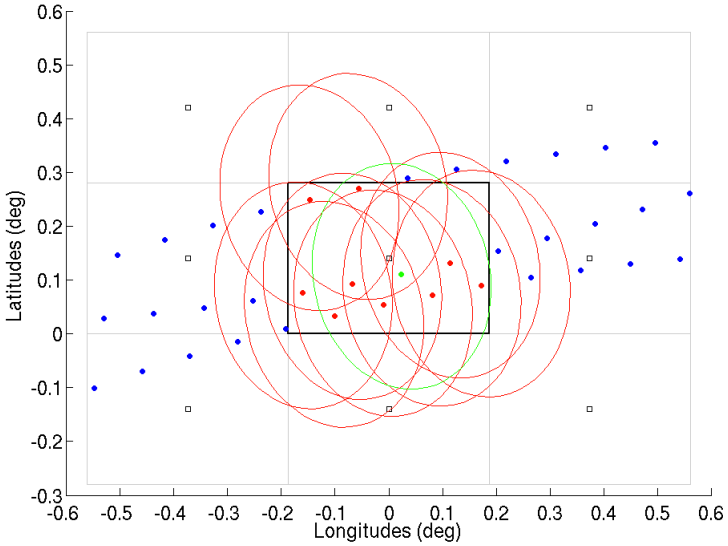

Figure 7. For a given radiometer sampling period (~12 ms in this example), the L1B_TB data samples (blue, red, and green dots) trace out a helical scanning pattern on the Earth surface. Data samples that fall into a grid cell (red and green dots) include T_B contributions from a significantly larger region than the grid cell (see text for description of color-coding).

[1] The 3-dB beam and main beam represent, respectively, approximately 52% and 89% of the total beam integrated power.

Of the many interpolation algorithms that have appeared in the literature three algorithms have been popular within the passive microwave remote sensing community. They are (1) drop-in-bucket, (2) nearest neighbor, and (3) inverse-distance-squared. These algorithms are described briefly in the following sections. Although there are other more advanced interpolation methods such as the Backus-Gilbert, SIR, and cubic convolution approaches [10-12], these methods require more complicated calculations and antenna pattern analyses, with no clear benefits over the simpler methods in addressing specific SMAP data product requirements. These methods are therefore not considered further for SMAP.

4.1 Drop-in-Bucket

In the Drop-in-Bucket (DIB) method, all T_B data samples that fall within a grid cell are averaged uniformly (i.e., equal weighting). If there are N data samples $\{T_{B1}, T_{B2}, T_{B3}, \ldots, T_{BN}\}$ within the cell, the corresponding gridded T_B can be expressed as:

$$T_{Bg} = \frac{1}{N}\sum_{i=1}^{N} \alpha_i T_{Bi} \quad (1)$$

where all α_i are equal to 1. Individual data samples exhibit random fluctuations that include thermal noise of the instrument. The averaging process reduces these fluctuations and results in a "cleaner" gridded T_B. This characteristic of DIB may be desirable for geophysical retrieval purposes as smaller T_B errors are usually associated with smaller retrieval errors. However, this approach results in considerable broadening of the effective antenna pattern of the grid cell due to equal weighting of all points in the cell, including those that could lie close to the grid cell boundaries. The resulting gridded T_B thus includes significant radiance contributions from outside the cell.

4.2 Nearest Neighbor

In the Nearest Neighbor (NN) method, each grid cell is assigned the value of the nearest T_B data sample nearest to the grid cell center (e.g. the green dot in Fig. 6). If there are N data samples $\{T_{B1}, T_{B2}, T_{B3}, \ldots, T_{BN}\}$ around a grid cell center, the corresponding gridded T_B can be expressed as:

$$T_{Bg} = T_{Bj} \quad (2)$$

where T_{Bj} represents the one data sample that is radially closest to the grid cell center.

Because only one data sample is used in NN interpolation, the resulting gridded T_B retains the same instrument-related random fluctuations as the input data (i.e., no reduction in noise by averaging). However, the broadening of the effective antenna pattern of the grid cell is relatively narrow (though displaced from grid center) since only a single sample antenna pattern, relatively close to the grid cell center, contributes to the resulting gridded T_B.

4.3 Inverse-Distance Squared

Another popular method for interpolating irregularly spaced data samples to a grid is the Inverse-Distance Squared (IDS) approach [14] that has often been used in microwave radiometry applications. The method operates on the assumption that data samples closer to a grid cell center should represent the value at that location more accurately than those that are further away. In IDS interpolation, all T_B data

samples that fall within a grid cell[2] are averaged non-uniformly, with weights varying inversely with the square of the radial distance between the data samples and the grid cell center:

$$T_{Bg} = \frac{1}{A}\sum_{i=1}^{N} \alpha_i T_{Bi} \tag{3}$$

where

$$A = \sum_{i=1}^{N} \alpha_i \tag{4}$$

$$\alpha_i = \frac{1}{d_i^2} \tag{5}$$

and d_i is the great-circle distance between the data sample T_{Bi} and the grid cell center, and is given by:

$$d_i = R_E \arccos[\sin\emptyset_i \sin\emptyset_o + \cos\emptyset_i \cos\emptyset_o \cos(\lambda_i - \lambda_o)] \tag{6}$$

Here, (ϕ_i, λ_i) and (ϕ_o, λ_o) are the latitudes and longitudes of the data sample i and grid cell center o, respectively. R_E (6378 km) is the radius of the Earth.

Inverse-distance-squared weighting can be considered as intermediate between DIB and NN in terms of effective antenna pattern and noise performance. It is also a more general formulation in the sense that the radius of influence is an additional parameter that can be used to optimize the weighting scheme.

4.4 T_B Quality Flags

As described in the L1B_TB data product specification document [19] there are four two-byte integer quality flags, one for each T_B channel data value:

- T_h quality flag
- T_v quality flag
- T_3 quality flag
- T_4 quality flag

When converted to binary representation, each T_B quality flag contains a series of 1's and 0's that indicate the quality of a particular T_B data value output as a result of the L1B_TB processing. The bit pattern and meaning of these flags can be found in the L1B_TB data product specification document [19].

In the L1C_TB processing, the quality flags of T_B data samples that fall within a given grid cell are logically 'OR'ed together on a bit-by-bit basis. The combined results are stored separately for the fore- and aft-directions in each EASE-Grid 2.0 projection data group.

4.5 Evaluation Criteria

In evaluating different interpolation methods it is necessary to formulate certain criteria for preferring one method to another. On this subject, two metrics have often appeared in the literature [13]: resolution

[2] In principle, the boundary of influence could be extended to a larger radius from the grid cell center.

and noise. An optimal interpolation method should introduce the least amount of resolution degradation to the original data, while adding as little noise as possible.

To evaluate the resolution degradation introduced by each interpolation method, two-dimensional antenna patterns were first generated at individual boresight locations that fall within a given 36-km EASE-Grid cell at different latitudes. The patterns were then superimposed according to DIB, NN, and IDS to produce corresponding effective antenna patterns. Figure 8 illustrates the fields of view (FOVs) of the effective antenna pattern at different power levels (−3 dB [magenta], −6 dB [green], −10 dB [blue], and −20 dB [black]) around 30°N. Shown also is the 36-km EASE-Grid cell under consideration. It is evident that while the 3-dB FOV dimension is comparable to that of the cell, the main-beam FOV dimension (approximated by the 20-dB FOV) is not.

The computed dimensions[3] of the FOV contours are shown in Table 4. Note that the NN antenna pattern has the same shape and size as an individual sample since there is no smoothing and broadening of the pattern due to sample averaging. However there is no noise-reduction afforded by NN. The noise of the observing instrument must be taken into account, however, in determining an optimal interpolation method; this aspect is examined below.

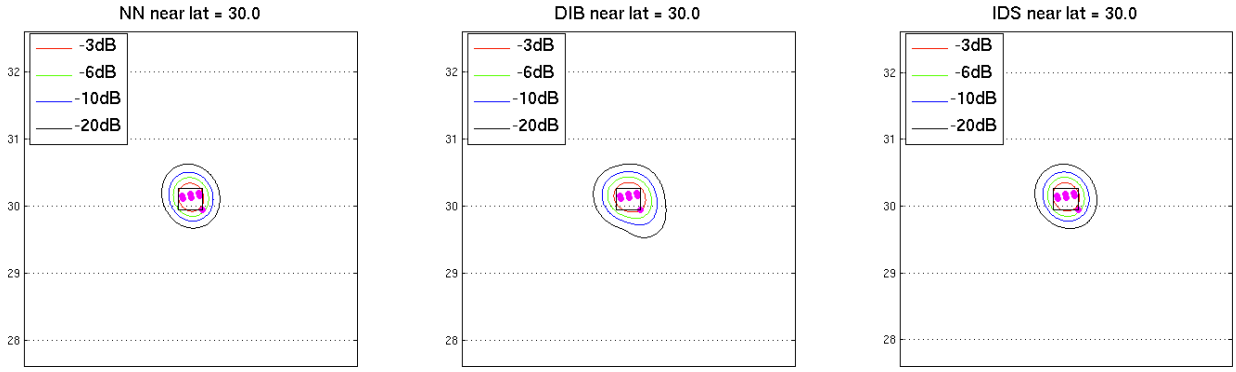

Figure 8. Variability in spatial extent of the effective antenna gain pattern at different power levels. The main-beam FOV, which captures about 89% of the energy observed by the radiometer, covers roughly 9 times more area than what a 36-km EASE-Grid cell represents.

Table 4: Effective antenna patterns can be computed by weighting individual patterns of multiple samples within a grid cell according to the interpolation method. The effective antenna pattern FOV dimensions for DIB, NN, and IDS as a function of latitude are shown.

	DIB		NN		IDS	
Latitude (Deg)	3-dB beam FOV size (km)	Main-beam FOV size (km)	3-dB beam FOV size (km)	Main-beam FOV size (km)	3-dB beam FOV size (km)	Main-beam FOV size (km)
0	42.0	99.0	36.7	83.5	38.8	91.4
5	42.0	98.9	36.7	83.5	38.6	90.5

[3] In most cases the FOVs are not symmetric. Here, the *square root* of the FOV area is used to depict the size of the FOV, in accordance with the L2-SR-285 entry in the SMAP Level 2 science requirements.

10	42.6	97.3	36.7	83.5	38.4	89.5
15	44.8	103.5	36.7	83.5	42.2	100.9
20	45.3	104.1	36.7	83.5	42.6	101.7
25	43.1	102.0	36.7	83.5	41.0	99.1
30	58.5	99.2	36.7	83.5	37.5	86.8
35	41.6	98.4	36.7	83.5	38.4	90.0
40	44.2	101.4	36.7	83.5	42.4	100.1
45	39.8	92.0	36.7	83.5	37.1	84.8
50	39.8	92.1	36.7	83.5	37.2	85.0
55	44.3	101.2	36.7	83.5	42.7	99.6
60	45.4	100.9	36.7	83.5	43.5	99.6
65	47.9	107.1	36.7	83.5	40.0	97.0
70	57.7	117.9	36.7	83.5	39.6	100.5
75	57.8	126.5	36.7	83.5	37.3	89.9
Average	**46.0**	**102.6**	**36.7**	**83.5**	**39.9**	**94.1**

To assess the trade-off between noise and resolution we can calculate the reduction in noise of the samples due to gridding for the three methods. If σ^2 represents the noise variance of the individual samples, then the corresponding effective noise variance σ_{eff}^2 of the gridded T_B will be given by:

$$\sigma_{\text{eff}}^2 = \frac{\sigma^2 N}{N^2} = \frac{1}{N}\sigma^2 \quad \text{(Drop-in-Bucket)} \tag{7}$$

$$\sigma_{\text{eff}}^2 = \sigma^2 \frac{\sum_{i=1}^{N} \alpha_i^2}{\left(\sum_{i=1}^{N} \alpha_i\right)^2} \quad \text{(Inverse-Distance Squared)} \tag{8}$$

where,

$$\alpha_i = \frac{1}{d_i^2}$$

$$\sigma_{\text{eff}}^2 = \sigma^2 \quad \text{(Nearest Neighbor)} \tag{9}$$

A simulation was performed of the SMAP orbital sampling, so that representative locations of SMAP radiometer TB samples falling within each grid cell globally were determined. Then the noise variances were computed according to the above expressions for each grid cell globally and then averaged over all grid cells for each method. The results, where σ_{eff} = square-root of the effective noise variance, are shown in Table 5. A value of σ = 0.51 K has been assumed as the representative NEDT of an individual radiometer sample.

Table 5: Resolution and noise characteristics of NN, DIB, and IDS.

Interpolation Method	3-dB Footprint Size	Main-beam Footprint Size	σ_{eff}
Drop in Bucket	46.0 km	102.6 km	0.18 K
Inverse-Distance Squared	39.9 km	94.1 km	0.31 K
Nearest Neighbor	36.7 km	83.5 km	0.51 K

The noise versus resolution characteristics are summarized in Fig. 9. As would be expected the inverse-distance-squared method provides a balance between noise (0.31K) and resolution (40 km). For this reason it was selected as the baseline gridding method for the L1C_TB product.

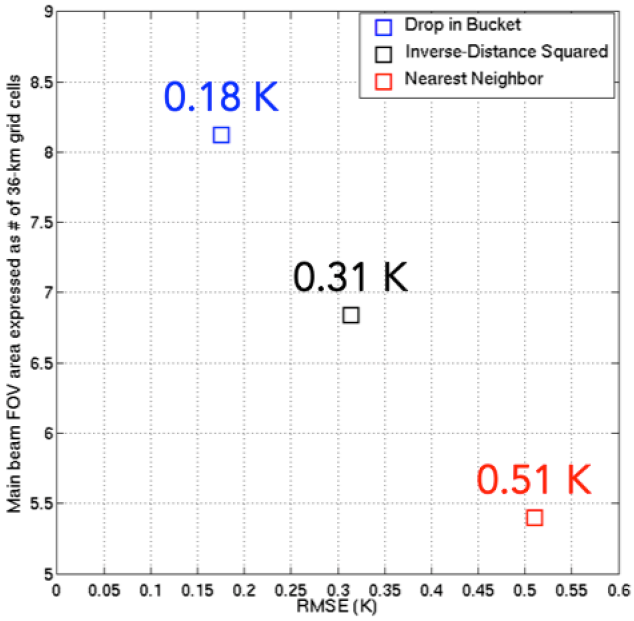

Figure 9. Noise-versus-resolution trade-off among the three gridding methods.

5. Post-Launch Cal/Val

During the post-launch Cal/Val period the performance of the L1C_TB product relative to the L1B_TB product will be evaluated in a number of ways. These include:

- Comparing images and examining differences between the two products over coastlines and other discrete boundaries, and heterogeneous terrain (lakes, mountains, rivers).
- Comparing T_B and T_B-gradient histograms of the two products over regions of varying heterogeneity (as above).
- Performing the above comparisons with both the baseline and alternate gridding methods to confirm the preferred baseline algorithm.

6. Algorithm Interfaces

6.1 Input Interface

It is assumed that the input L1B_TB granules will contain ascending or descending half-orbit of data. A typical L1B_TB granule contains radiometric brightness temperature values, as well as their associated time tags, geolocation data, incidence angles, azimuth angles, reflected sun angles, and quality flags as described in [1].

6.2 Output Interface

The L1C_TB data product will be available in ascending or descending half-orbit of data. Each granule contains data fields (see Table 1) acquired in both fore- and aft-look scans. The output files will be written in HDF5 format.

6.3 Ancillary Data Interface Assumptions

No external ancillary data other than the center latitude/longitude coordinates of EASE-Grid cells are required for the generation of the L1C_TB data product.

7. CPU and Data Volume

Because the processing is computationally simple for all the candidate algorithms they can be handled with ease by most modern computing platforms, such as those operated by the SMAP SDS.

As far as data volume is concerned, the requirements will be minimal by modern storage standards. A typical L1B_TB half-orbit granule is expected to cover an area of 1,000 km (swath width) times ($2\pi \times 6{,}378$) / 2, or 2×10^7 km^2. This area consists of about 2×10^7 / (36×36), or 15,000 36-km grid cells. With $K \sim 15{,}000$ in Table 3, each half-orbit granule takes up about ($1 \times 8 + 1 \times 24 + 26 \times 4$) × 15,000 × 2 × 3 ~ 11.7 MB. As there are about (365/8 × 117) = 5,338 full orbits per year, the total annual data volume for the L1C_TB data product is expected to be 5,338 × 11.7 × 2 = 122.0 GB (ascending and descending granules included).

References

[1] SMAP Algorithm Theoretical Basis Document: *L1B Radiometer Product*. SMAP Project, GSFC SMAP-006, NASA Goddard Space Flight Center, Greenbelt, MD.

[2] National Research Council, "Earth Science and Applications from Space: National Imperatives for the Next Decade and Beyond," pp. 400, 2007.

[3] D. Entekhabi, E. Njoku, P. Houser, M. Spencer, T. Doiron, J. Smith, R. Girard, S. Belair, W. Crow, T. Jackson, Y. Kerr, J. Kimball, R. Koster, K. McDonald, P. O'Neill, T. Pultz, S. Running, J. C. Shi, E. Wood, and J. van Zyl, "The Hydrosphere State (HYDROS) mission concept: An Earth system pathfinder for global mapping of soil moisture and land freeze/thaw," IEEE Trans. on Geosci. and Remote Sensing Trans. on Geosci. and Remote Sensing, vol. 42(10), pp. 2184-2195, 2004.

[4] Entekhabi, D., E. Njoku, P. O'Neill, K. Kellogg, W. Crow, W. Edelstein, J. Entin, S. Goodman, T. Jackson, J. Johnson, J. Kimball, J. Piepmeier, R. Koster, K. McDonald, M. Moghaddam, S.

Moran, R. Reichle, J. C. Shi, M. Spencer, S. Thurman, L. Tsang, J. Van Zyl, "The Soil Moisture Active and Passive (SMAP) Mission", Proceedings of the IEEE, 98(5), 2010.

[5] NSIDC, *EASE-Grid Data*, [Online] Available: http://nsidc.org/data/ease/index.html [Accessed: Aug 25, 2011].

[6] Dunbar, S. and S. Chan (2009): *SMAP Fixed Earth Grids,* SMAP Science Document, May 2009.

[7] Dunbar, S. (2009): *Application of the Space Oblique Mercator Projection to SMAP*, SMAP Science Document, January 2009.

[8] SMAP Algorithm Theoretical Basis Document: *L1B and L1C Radar Products*. SMAP Project, JPL D-53052, Jet Propulsion Laboratory, Pasadena, CA.

[9] SMAP Level 2 Science Requirements. SMAP Project, JPL D-45955, Jet Propulsion Laboratory, Pasadena, CA.

[10] Poe, G. A. (1990): Optimum interpolation of imaging microwave radiometer data, *IEEE Trans. Geosci. Rem. Sens., 28(5),* pp. 800-810.

[11] Early, D. S. and D. Long (2001): Image Reconstruction and Enhanced Resolution Imaging from Irregular Samples, *IEEE Trans. Geosci. Rem. Sens., 39(2),* pp. 291-302.

[12] Gu, H. and A. W. England (2007): AMSR-E Data Resampling With Near-Circular Synthesized Footprint Shape and Noise/Resolution Tradeoff Study, *IEEE Trans. Geosci. Rem. Sens., 45(10),* pp. 3193-3203.

[13] Knowles, K: *Intercomparison of resampling methods for SMMR Pathfinder in EASE-Grid*, [Online] Available: http://geospatialmethods.org/smmrpfreport/ [Accessed: Aug 25, 2011].

[14] Shepard, D. (1968): A two-dimensional interpolation function for irregularly-spaced data, *Proceedings of the 1968 ACM National Conference*, pp. 517–524.

[15] NSIDC, *Nimbus-7 SMMR Pathfinder Daily EASE-Grid Brightness Temperatures*, [Online] Available: http://nsidc.org/data/docs/daac/nsidc0071_smmr_ease_tbs.gd.html [Accessed: Aug 25, 2011].

[16] NSIDC, *DMSP SSM/I-SSMIS Pathfinder Daily EASE-Grid Brightness Temperatures*, [Online] Available: http://nsidc.org/data/nsidc-0032.html [Accessed: Aug 25, 2011].

[17] NSIDC, *AMSR-E/Aqua Daily EASE-Grid Brightness Temperatures*, [Online] Available: http://nsidc.org/data/nsidc-0301.html [Accessed: Aug 25, 2011]

[18] Data Product Specification for L1C_TB Data Product, SMAP Project Document.

[19] Data Product Specification for L1B_TB Data Product, SMAP Project Document.

[20] Brodzik M.J., Billingsley B., Haran T., Raup B., Savoie M.H. *EASE-Grid 2.0*: Incremental but Significant Improvements for Earth-Gridded Data Sets. *ISPRS International Journal of Geo-Information*. 2012; 1(1):32-45.

[21] NSIDC, *EASE-Grid Data, Frequently Asked Questions*, [Online] Available: http://nsidc.org/data/ease/faq.html [Accessed: May 22, 2012]